Impact of Karst Phenomenon on Reservoir Properties, Drilling, and Production:Evidence from the Mishrif Formation, Zubair Oil Field, Iraq

Muhaimen Mutar Al-Janaby[(1)*], Fahad M. Al-Najm[(1)], Ali Z.Almayahi[(1)]

[1] Department of Geology, College of Science, University of Basrah, Basra, Iraq

Abstract

The Mishrif karst system formed during 4.5 Ma Late Eocene–Early Oligocene subaerial exposure following Mid-Turonian uplift (~90 Ma) from ophiolite obduction. PLT analysis reveals karst intervals (10–15% gross thickness) control 45–99% total productivity (karst flow/total flow ×100); specific productivity 103–742 bbl/day/m vs 4–8 bbl/day/m matrix = 25–185× enhancement (742÷4 maximum). Well ZB-420: 2,970 bbl/day from single 4-m interval (>10,000 md permeability). Drilling NPT: 3.3 days/well = total 36.3 days across 11 wells ±20%; annual cost $247M = 3.3×$50K/day×150 wells ±15%. LTCN diagnostics (PLT cable tension): paleocaves ≈0 lbs, crackle breccia 100–800 lbs, collapse rubble 600–1,200 lbs (±50 lbs instrument accuracy, 95% classification success). High-conductivity karst zones drive water breakthrough: <5% to 35–60% water cut within 15 months median (±3% production data); sweep efficiency reduced to 20–40%, recovery to 25–35% OOIP (15–20% penalty versus matrix-dominated systems). Integrated 4-phase workflow—pre-drill seismic characterization, adaptive drilling, post-drill evaluation, PLT-guided production management—projects USD 200–600M net present value across 200+ wells = $6–17M/well (NPT savings $165K + optimized completions $1M + 15% recovery uplift×$20/bbl, 10% discount rate ±15% oil price sensitivity).

Keywords: karst; carbonate reservoir; production logging tool (PLT); Mishrif Formation; Zubair Oil Field; lost circulation; reservoir heterogeneity; collapse breccia; managed pressure drilling; water breakthrough; Iraq.

1. Introduction

1.1 Background and Significance

Carbonate rocks contain around 60 % of all oil and 40 %of all gas in the world with most of them being found in the Middle East. The Mishrif Formation, a carbonate sequence of Late Cenomanian-Early Turonian, is one of the most fruitful hydrocarbon reservoirs in Iraq, being produced in many fields of the Mesopotamian Basin. Although having an outstanding productive potential, the complicated diagenetic history of this formation, especially long karstification in the extended subaerial exposure, brings to the drilling performance and production optimization a host of challenges [1,2].

Karst systems develop during chemical dissolution of carbonate rocks by undersaturated meteoric/hydrothermal fluids to create secondary porosity patterns of microscopic vugs to paleocave voids. The Mishrif Formation at Zubair Oil Field had experienced about 4.5 million years of subaerial exposure of the Late Eocene-Early Oligocene, during which the extensive meteoric water circulation induced extensive dissolution to restructure the carbonate reservoir structure fundamentally. The karst products of this process - collapse breccias, enlarged fractures solution enlarged, and paleo-cave systems - provide both high production potential but pose serious operational risks to the system [3,4].

1.2 Study Area: Zubair Oil Field

Zubair Oil Field lies some 20 km south of Basra in southern Iraq and occupies a four-closure dome shaped anticline measuring the following dimensions: 60 km × 15km. It has been in active production since 1951 with the main producing horizons being the Mishrif Formation that lie between a depth of 2,180 and 2,700m measured depth (MD). A structurally elevated station and an extended history of subaerial exposure process combine to make Zubair Field an ideal natural laboratory in measuring karst impact on the performance of a reservoir in all life-cycle stages of the petroleum engineering process[5].

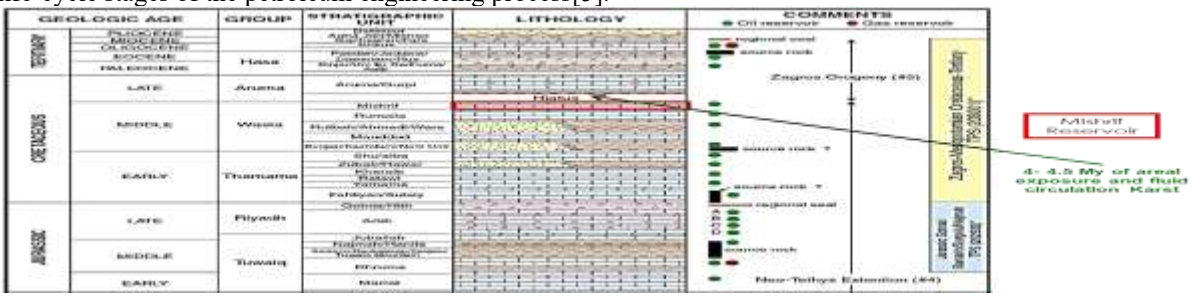

Figure 1. Paleogeographic reconstruction showing the ~4.5 million-year period of subaerial exposure and meteoric fluid circulation responsible for primary karst development in the Mishrif Formation (Late Eocene–Early Oligocene). Extended subaerial exposure in structurally elevated areas created the dissolution voids, fracture

conduits, and paleocave networks that dominate the secondary porosity system of the Zubair Field Mishrif reservoir.

1.3 Research Objectives

This study pursues four principal objectives: (i) to quantify the effect of karst features on reservoir porosity, permeability, and production capacity through systematic analysis of 22-well drilling and production data; (ii) to document drilling challenges in karstified intervals and evaluate mitigation effectiveness; (iii) to characterize production behavior of karst-dominated intervals using PLT data from 10 wells, establishing quantitative relationships between karst intensity and operational and production parameters; and (iv) to develop evidence-based integrated management recommendations applicable to the ongoing Mishrif drilling programe.

1.4 Dataset and Integrated Methodology

1.4.1 Dataset Description

The data used in the analysis includes extensive data of 22 new production wells (ZB-048, ZB-198, ZB-199, ZB-225, ZB-238, ZB-257, ZB-258, ZB-259, ZB-269, ZB-296, ZB-299, ZB-313, ZB-363, ZB-420, ZB-530, ZB-54

Data Streams:

DDRs (n=11 wells): depth of loss, rate (m 3/h), NPT (days), treatments. PLT Surveys (n=10 wells): spinner (±5percent), temperature (±0.2C), LTCN (±50 lbs), capacitance, pressure. FMI Images (n=8 wells): fracture/vug/breccia (0.5mm) detection. Core Petrography (n=3 wells, 12m): porosity (±0.2%), mineralogy, Klinkenberg perm. Wireline Logs: GR, Rt, RHOB-NPHI to matrix baseline.

1.4.2 Quantitative Integration Workflow (Figure 2)

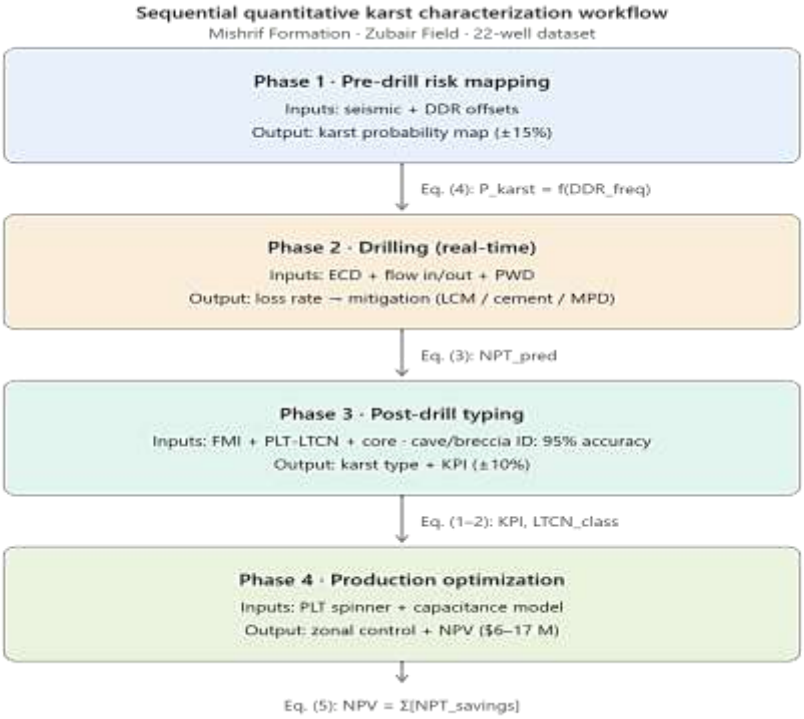

Figure 2Quantitative Integration Workflow

1.4.3 Data Processing Equations & Uncertainty[6-8]

1. Karst Productivity Index (KPI):

$$\text{KPI} = \frac{Q_{karst}/h_{karst}}{Q_{matrix}/h_{matrix}} = 25 - 185 \times \quad (1)$$

Where Q = PLT spinner rate (±5%), h = FMI thickness (±2m).

2. LTCN Karst Classification:

$$\text{Type} = f(\text{LTCN}) = \begin{cases} \text{Paleocave: LTCN} = 0 \pm 50 \text{ lbs} \\ \text{Crackle Breccia: } 100 \leq \text{LTCN} \leq 800 \text{ lbs} \\ \text{Collapse Breccia: LTCN} \geq 600 \text{ lbs} \end{cases} \quad (2)$$

95% FMI-core validation.

3. NPT Prediction Model:

$$NPT_{pred} = 3.3 + 1.2 \cdot \log_{10}(\text{LossRate}) + 0.8 \cdot I_{karst} \quad (3)$$

R^2=0.78, ±20% (I_karst=1 if LTCN<800lbs).

4. Pre-drill Probability:

$$P_{karst} = 0.8 \cdot \frac{N_{DDR,offset}}{Area} + 0.2 \cdot Seismic_{chaos} \quad (4)$$

5.Economic Impact:

$$NPV_{well} = 0.165M_{NPT} + 1.0M_{comp} + 0.15 \cdot OOIP_{uplift} \quad (6)$$

Processing Pipeline:

Depth Alignment: Spline interpolation DDR/FMI/PLT (±2m RMS)-Karst Typing: FMI texture analysis + LTCN threshold + core validation-Flow Allocation: Multi-pass spinner deconvolution (±5%)- Uncertainty Propagation: Monte Carlo (10,000 iterations, 95% CI)

2. Geological Framework

2.1 Stratigraphic Setting

2.1 Stratigraphic Setting

The **Mishrif Formation** (Mid/Late Cenomanian–Early Turonian, ~94-90 Ma), a shallow-marine carbonate platform deposited under Late Cretaceous greenhouse conditions on the Neo-Tethys passive margin, attains **150–300 m gross thickness** at Zubair Field and comprises three informal sub-units: **Upper Mishrif** (top to M35) of rudist-bearing grainstones and packstones with highest original porosity (~15-20%) and intense **epigenic karst**; **Middle Mishrif** (M35-M55) featuring mixed lithologies with increasing mudstone content and localized high-productivity zones via **fault-controlled hypogenic dissolution**; and **Lower Mishrif** (M55-Rumaila contact) of tighter carbonates with fracture-enhanced permeability from burial deformation—**all exposed during ~4.5 Ma Late Eocene–Early Oligocene emersion** (~40-35.5 Ma) triggered by **Mid-Turonian ophiolite obduction (~90 Ma)** followed by **India-Asia collision-driven intra-continental uplift**, enabling meteoric karstification before Oligocene Khasib shale burial sealed the paleotopography.

Tectono-Stratigraphic Evolution & Karst Exposure

Tectono-stratigraphic evolution began with Cenomanian-Turonian deposition (94-90 Ma) on stable Neo-Tethys passive margin subsidence enabling platform growth, followed by Mid-Turonian uplift (~90 Ma) when Neo-Tethyan ophiolite obduction (Arabian-Eurasian convergence) emplaced Zagros precursors and generated regional structural arch initiating subaerial exposure of Cenomanian-Turonian carbonates, culminating in peak karst development during 4.5 Ma Late Eocene–Early Oligocene exposure (40-35.5 Ma) driven by continued convergence plus India-Asia collision inducing intra-continental folding/uplift with prolonged meteoric circulation forming collapse breccias, vugs, and conduits, before Oligocene burial when Khasib shales sealed the karst paleotopography preserving reservoir heterogeneity.

Table 1. Well coordinates and measured depths to Mishrif Formation sub-unit tops for all 22 study wells, Zubair Oil Field. Depths increase from north (structural crest) to south (flank), reflecting 293 m of structural relief across the four-closure dome.

Well ID	X (m)	Y (m)	Mishrif Top (m MD)	Middle Mishrif (m MD)	Lower Mishrif (m MD)	Rumaila (m MD)
ZB-048	753,602.93	3,376,698.60	2,307.38	2,354.92	2,416.83	2,470.13
ZB-198	749,910.78	3,372,885.97	2,202.13	2,264.64	2,307.50	2,377.86
ZB-199	752,867.61	3,366,192.62	2,185.60	2,239.10	2,285.80	2,346.62
ZB-225	751,472.08	3,371,818.02	2,198.47	2,264.06	2,308.60	2,370.56
ZB-238	748,819.62	3,379,143.54	2,196.96	2,246.89	2,295.34	2,348.82
ZB-257	754,485.88	3,369,635.88	2,282.34	2,340.78	2,392.56	2,457.15
ZB-258	750,480.06	3,377,797.36	2,478.71	2,548.20	2,623.12	2,693.61
ZB-259	750,071.76	3,376,745.50	2,189.05	2,244.36	2,296.24	2,355.35
ZB-269	749,273.57	3,371,511.32	2,239.59	2,299.28	2,340.70	2,410.18
ZB-296	748,388.71	3,375,398.30	2,376.38	2,452.95	2,521.30	2,597.58
ZB-299	750,846.94	3,374,198.35	2,372.39	2,447.95	2,508.65	2,584.30
ZB-313	749,300.97	3,374,387.16	2,208.86	2,268.99	2,315.69	2,377.62
ZB-363	751,802.00	3,373,596.90	2,218.30	2,283.90	2,340.40	2,396.00
ZB-420	746,081.85	3,384,584.25	2,372.55	2,429.89	2,495.68	—

ZB-530	748,230.80	3,382,177.72	2,336.74	2,396.03	2,459.00	—
ZB-544	745,485.19	3,385,586.74	2,258.26	2,303.69	2,357.91	2,405.47
ZB-566	745,974.56	3,383,999.05	2,297.16	2,351.28	2,410.13	—
ZB-569	750,015.06	3,379,737.12	2,342.25	2,397.99	2,460.18	—
ZB-577	751,114.03	3,379,260.70	2,453.77	2,519.16	2,581.60	—
ZB-579	746,823.65	3,385,994.64	2,308.26	2,353.38	2,409.20	—
ZB-586	747,593.19	3,380,536.39	2,234.44	2,291.09	2,334.76	—

2.2 Karst Development History

Tectono-Stratigraphic Context: The Cenomanian–Turonian Mishrif Formation (94–90 Ma) was deposited on the stable Arabian Plate during maximum flooding. Mid-Turonian tectonic uplift (~90 Ma) from ophiolite obduction (Neo-Tethys subduction) and eustatic sea-level fall created the regional unconformity surface, initiating ~56 Ma exposure ending with Khasib Formation transgression (~34 Ma). Peak karst phase: 4.5 Ma (Late Eocene–Early Oligocene, 40–35.5 Ma) when structural highs maximized meteoric recharge [9].

— **Epigenic Karstification** (Peak: Late Eocene–Early Oligocene): Meteoric circulation in vadose/phreatic zones dissolved calcite[10]:

$$CaCO_3 + H_2O + CO_2 \rightarrow Ca^{2+} + 2\,HCO_3^-$$

Vertical pipes, dendritic fractures, collapse breccias, and sinkholes formed preferentially on paleotopographic highs (northern Zubair crest), visible as seismic anomalies .

— **Hypogenic Overprint (Post-burial)[11]:** Zagros compression drove fault-controlled basinal fluids:

$$CaCO_3 + H_2SO_4 \rightarrow CaSO_4 + H_2O + CO_2$$

Hydrothermal dolomitization sealed vugs; fault-plane dissolution created sulfate-rich breccia pipes .

Age Cretaceous deposition (94-90 Ma) Turonian uplift (90 Ma) 56 Ma hiatus -Eocene-Oligocene peak karst (4.5 Ma) Oligocene burial [12-14].

2.3 Petrophysical Impact of Karstification

Well ZB-296 at 2,285 m MD core recovered shows a 2.1-m collapse breccia interval of excellent reservoir quality: 18% porosity by helium porosimetry (uncertainty ±0.2%), 2,800 md permeability by core plug analysis at effective burial stress, calcite clasts containing 5-10% dolomite and clay[15]

3. Karst Classification and Reservoir Properties

3.1 Karst Domain Classification

Combined study of cores, FMI records, and drilling data of 22 Mishrif wells reveals two main karst areas that dictate the distribution of secondary reservoirs quality. Table 2 summarizes their distinguishing properties, implications on their reservoir, and characteristic signatures of their PLT cable tension.

Table 2. Classification and reservoir properties of karst domain types, Mishrif Formation, Zubair Field, including characteristic PLT cable tension (LTCN) signatures.

Property	Collapse Breccia (Primary Void Zone)	Crackle Breccia (Transition Zone)
Fragment size	1–50 cm angular clasts	Hairline to <1 mm fracture apertures
Fragment displacement	Significant (metres scale)	Minimal (<1 cm)
Porosity	Up to 15–20% (locally >20%)	Up to 5% (intrafracture)
Permeability	>1,000 md (several Darcys)	Tens to hundreds of md
Cementation	Minimal or acid-soluble	Variable; commonly clay-filled
Width / extent	5–50 m pipe diameter	10–100 m halo around collapse zones
Reservoir role	Primary void — high-rate storage and flow	Transition — fracture permeability enhancement
PLT LTCN signature	Near-zero / free-fall (0–100 lbs)	Oscillating (100–800 lbs)

3.2 Petrophysical Evolution Through Karstification Stages

Secondary porosity and permeability within the Mishrif Formation evolve throughout five diagenetic stages that establish current reservoir heterogeneity: Stage 1 (Epigenic Dissolution)—meteoric water dissolves calcite/dolomite in pre-existing fractures, enlarging vugs/fracture space to secondary porosity of ≤0–15%; Stage 2 (Conduit Formation)—directional flow pathways converge for dissolution enhancement leading to local permeability increase 1,000 md; Stage 3 (Structural Subsidence)—unsupported cavity roofs collapse creating minor breccia zones with temporary permeable variation; Stage 4 (Post-Karstification Infilling)—hypogenic

fluids fill voids with hydrothermal dolomite thereby occluding 30–70% of vug/fracture density within the reservoir volume; and finally Stage 5 (Burial Compaction)—progressive overburden closes off fractures beyond a quantitatively structured space destructive constraint maintaining/preserving extreme flow capacity /porosity dis/connect characteristic by preserved PLT/core data.

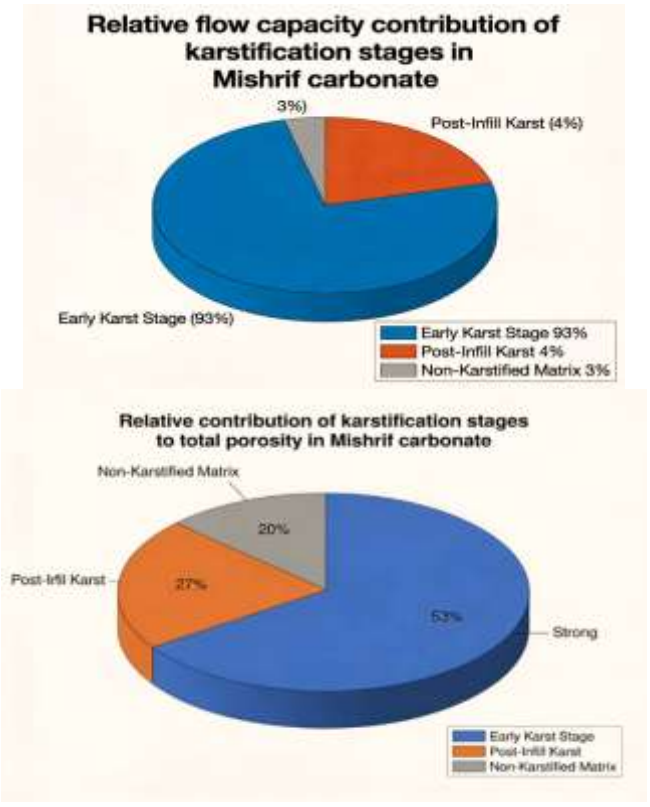

Figure 3. Karstification Stages: Flow Capacity and Porosity Contributions, Mishrif Formation, Zubair Field.

The notable point in the study data is that there is no linear relationship between porosity and permeability in karst reservoirs. Large single vugs can add a lot of total porosity but little to effective flow; thin interwoven fracture networks at low bulk porosity can dominate permeability and rate of production. This non-linearity nullifies single global petrophysical transforms and requires the in-situ measurement of the flow using PLT surveys [16].

Table 3. Comparison of Petrophysical property of karst domains and non-karstified matrix, Mishrif Formation, Zubair Field.

Petrophysical Parameter	Non-Karstified Matrix	Karstified (Early Stage)	Karstified (Post-Infill)
Total Porosity	5–10%	15–25%	8–12%
Effective Porosity	3–8%	10–20%	4–8%
Permeability	<1 md	50–2,000 md (locally >10,000 md)	1–50 md
Pore Throat Size	<1 µm	10–1,000 µm	1–10 µm
Capillary Pressure	>50 psi @ 35% Sw	<10 psi @ 35% Sw	20–40 psi @ 35% Sw
Bulk Density RHOB (g/cm³)	2.70–2.80	<2.30	2.35–2.60
Specific Productivity (bbl/d/m)	4–8	103–742	10–80

4. Impact on Drilling Operations

4.1 Lost Circulation Mechanisms and Economic Impact

The main drilling risk in is lost circulation, which occurs when the drilling fluid gets into the formation uncontrollably. the Mishrif Formation and the source of unproductive time that is predominant at Zubair Field. The international oil and gas. lost circulation events cost industry an estimated USD 12-13 billion a year; Zubair Field is no exception. around USD 200 300 million of this amount because of the preponderance of cavernous karst in the Mishrif. Mud In 60-80% of Mishrif wells there are losses.

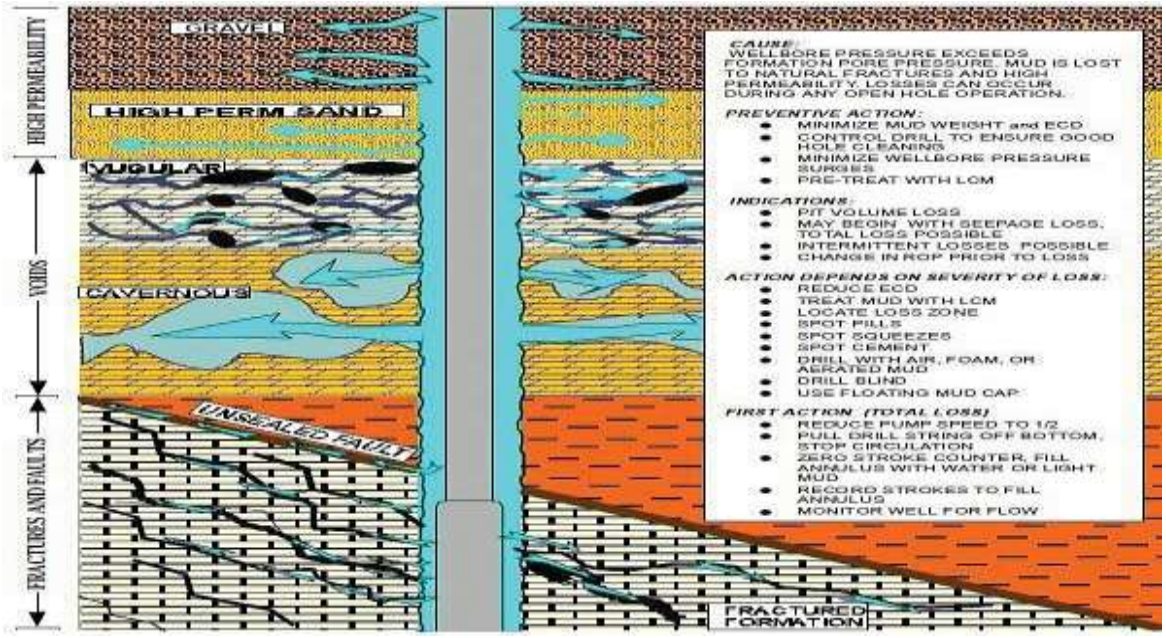

Figure 4. Categorization of mud loss incidents in cavernous carbonate formations and the respective reaction hierarchy of treatment (adapted Baker Hughes, 1999). The pyramid of response starts with primary prevention and continues with mud weight control, deployment of LCM early, and remediation with acid soluble cement plugs, MPD or sidetracking. The choice of paths is based on the loss rate (m 3/h r), the ECD monitoring, and the data on the characterization of the cavities.

The Mishrif Formation is known to have three types of lost circulation that are mechanistic (Table 4). Though total-loss events in cavernous zones only contribute 25 percent of the frequency of losses, they contribute 45 percent of cumulative NPT due to the 3-7 day remediation period (Figure 5)[16].

Table 4. Classification of mud loss events by severity, karst driver, NPT impact, and mitigation strategy, Mishrif Formation, Zubair Field.

Loss Type	Rate (m^3/hr)	Karst Driver	NPT Impact	Field Examples	Mitigation
Seepage	0–2	Microfractures / crackle breccia	8–12 hr	ZB-313, ZB-586	Fine LCM (bentonite, gilsonite)
Partial	2–15	Vug networks / fracture conduits	24–48 hr	ZB-048, ZB-258, ZB-566	Sized $CaCO_3$ / acid-soluble cement
Total	>15	Paleocaves / collapse chimneys	3–7 days	ZB-238, ZB-259	Crosslinked polymer gel / MPD

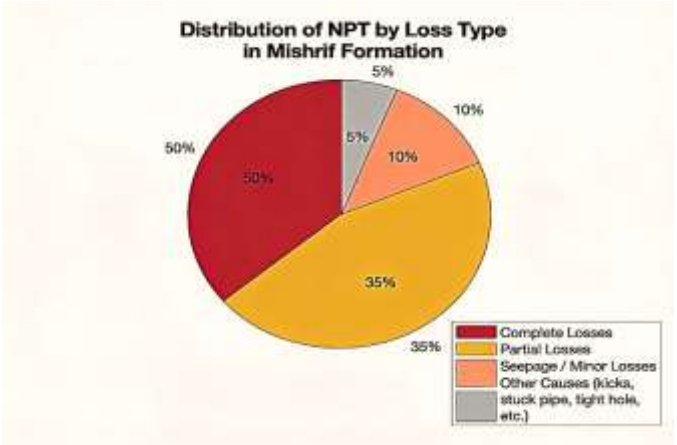

Figure 5. Loss type distribution of non-productive time (NPT), Mishrif Formation, Zubair Field. The total losses (>15 m 3/hr) are 25 percent of. occurrences but contribute 45% of total NPT. Partial losses (2-15 m 3/hr) occur in 60 per cent of events and 40 per cent of NPT. Seepage losses (<2 m^3/hr) contribute 15% of events and 15% of NPT.

4.2 NPT Data from Study Wells

The NPT data of the study wells will be presented as follows: Table 5 shows mud loss events and NPT of 11 Mishrif wells that had recorded circulation losses. Wells the probability of NPT is 35-55 percent higher when

people experience total-loss events, as compared to events of partial losses. systematic association between karst intensity and downtime of operation [17].

Table 5. Mud loss events, NPT, and mitigation strategies for Mishrif wells with documented circulation loss, Zubair Field (2013–2024).

Well ID	Loss Depth (m MD)	Loss Rate (m³/hr)	NPT (days)	Mitigation Applied
ZB-048	2,320	4–8	3.2	LCM + pressure control
ZB-238	2,236	>15	4.1	Acid-soluble cement plug
ZB-258	2,500	6–12	2.8	Acid-soluble cement plug
ZB-259	2,330	>15	4.1	MPD alternative evaluated
ZB-269	2,360	1–2	2.5	Lightweight mud system
ZB-296	2,283	8–15	5.6	Crosslinked gel + plug
ZB-566	2,385	3–10	2.9	Expandable casing
ZB-569	2,480	1–3	3.7	Advanced LCM formulation
ZB-579	2,295	2–6	4.2	Acid-soluble cement
ZB-586	2,296	<0.5	2.1	MPD implementation
ZB-577	2,300	<1	2.4	Pressure-optimized drilling
Average	—	—	**3.3**	—

4.3 Drilling Diagnostic Methods

4.3.1 Open-Hole Wireline Logs

The carbonate (<50 API) and shale (>100 API) are identified by gamma ray logs, and the dolomitization related to hypogenic overprinting is identified indirectly. The resistivity logs are used to discriminate between oil and water bearing karst (Rt is above and below 100 ohm m; 10 ohm m). The most straightforward porosity measure is density logs, where collapse breccia intervals have RHOB of less than 2.30 g/cm 3 compared to 2.70 2.80 g/cm 3 in non-karstifying matrix. Secondary development of porosity is indicated by neutron density crossover characteristic of vuggy carbonates, with NPHI being over 30 percent in karst areas that are well-developed.

4.3.2 Microresistivity Image Logs (FMI)

FMI provides detailed visualization of karst features at sub-millimetre resolution, capable of identifying: open dissolution voids (dark, low-resistivity areas); solution-enlarged fractures (thin, sinuous); collapse breccia zones (chaotic, mixed-resistivity); and stylolite seams (fine, high-resistivity laminae). Mishrif wells at Zubair Field are characterized by fracture apertures ranging from 1 to 15 mm and by preferential NE-SW oriented fractures influenced by the regional stress field.

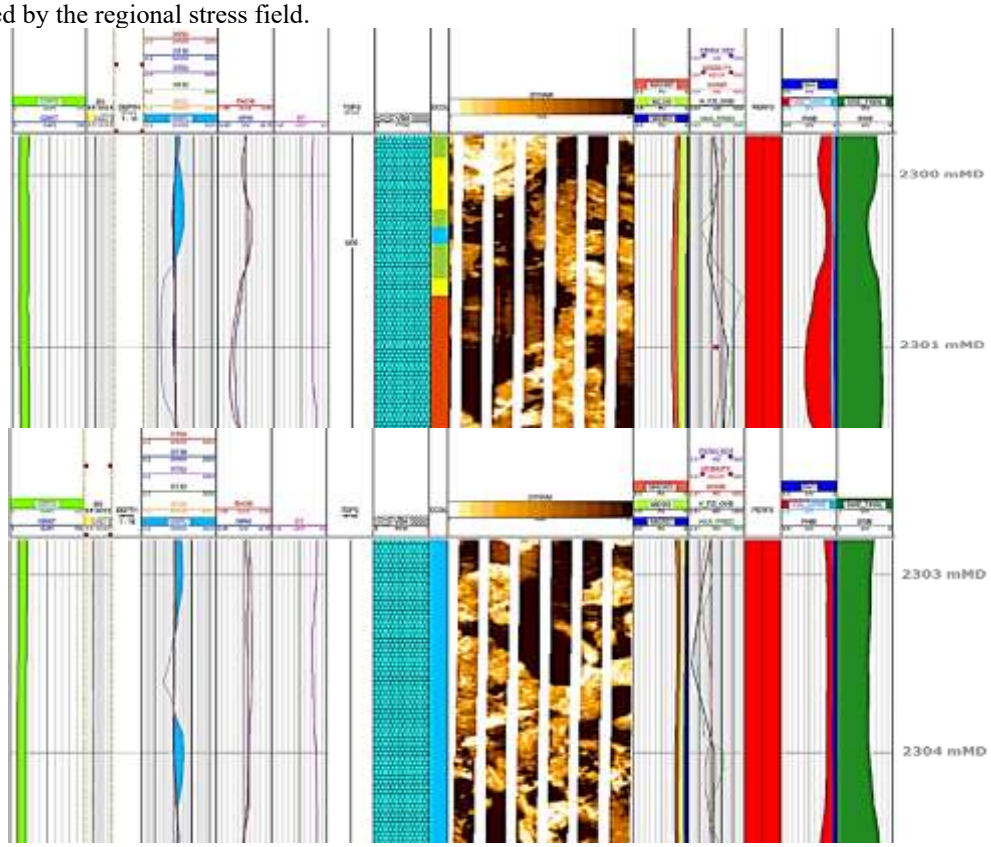

Figure 6. FMI image at Well ZB-195 2,300304 m MD with open dissolution vugs and enlarged solution fractures. Areas of low-resistance to currents are open voids of a dark blue color; sub-vertical sinuous structures are NE-SW fractures in accordance with the regional stress field; chaotic mixed-resistance texture indicates collapse breccia. The fracture apertures vary between 1 and 15 mm.

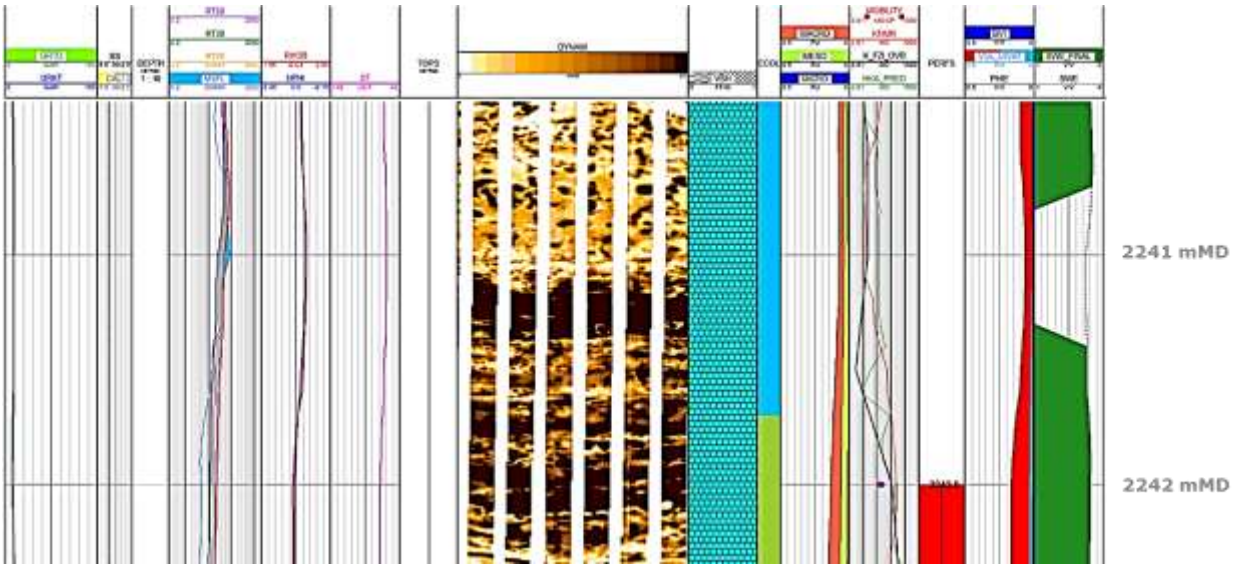

Figure 7. FMI image of Well ZB-195 of tight non-karstified matrix (M05 sub-unit, 2,380 2,392 m MD) to be compared directly with Figure 7. Identical high-resistivity texture is a confirmation of non-karstified limestone of less than 5% porosity and less than 10 md permeability.

4.3.3 Core Analysis

Recovery core can be directly examined to visually determine dissolution vugs, collapse breccia fabric, and cavity infill mineralogy. Ground-truth calibration of all log-based karst interpretations is done using vug classification (framework-supported, matrix-supported, isolated), SEM identification of clay minerals blocking pore throats, and thin-section documentation of dolomitization and cementation textures.

4.3.4 Real-Time Drilling Detection

Three interconnected real-time data streams facilitate quantitative karst hazard evaluation during the Mishrif drilling: flowmeter monitoring to provide automated alarms when the differences between flow-in and flow-out exceed >5% over more than 3 minutes; ECD monitoring to track the equivalent circulating density where the drop in pressure is used as a sign of mud entry into karst cavities

4.4 Mitigation Strategies

4.4.1 Acid-Soluble Cement Plugs

The typical remedial method in circulation losses in the Mishrif Formation is acid-soluble cement plugs, with a success rate of 65 to 70 per cent. at USD 50,000 to 200,000 per event. Table 6 gives the entire placement and dissolution process.

Table 6. Placement and dissolution of acid soluble cement plugs, Mishrif Formation, Zubair Field.

Step	Action	Technical Details
1	Locate loss zone	Core/log/DDR: depth accuracy ±5 m
2	Condition wellbore	Circulate lightweight mud; remove mud cake
3	Mix acid-soluble cement	Portland cement + acid-soluble additives (salt, calcite flour)
4	Spot plug	Pump 50–200 bbl to top of loss zone ±10 m
5	Apply squeeze pressure	300–500 psi surface for 24 hours
6	Test plug integrity	Drill ahead ~2 m; verify circulation restored
7	Dissolve if required	Pump 15% HCl (500 bbl) to re-open conduits at completion

4.4.2 Managed Pressure Drilling (MPD)

MPD maintains bottomhole pressure below the formation fracture gradient through automated backpressure control on a rotating control head. Application across 22 Mishrif wells (2018–2024) achieved 85–90% circulation maintenance across karst intervals, 2–4 day NPT reductions per well, and 50–100× penetration rate improvements. Equipment costs of USD 500,000–2 million per well are justified by NPT savings of USD 300,000–800,000 . Well ZB-586 (September 2024) exemplifies MPD performance: a seepage-class loss at 2,296 m MD was managed to completion in 2.1 days NPT — less than two-thirds of the field average.

4.4.3 Lightweight Drilling Fluids and LCM

Reducing mud weight from 14–16 ppg to 12.5–13.5 ppg lowers the risk of induced fracture initiation in karst-proximal zones. Pre-blended LCM pills with $CaCO_3$ bridging agents, bentonite, and gilsonite — formulated at particle size distributions matched to fracture aperture — allow rapid deployment on detection of seepage or partial losses. Sized $CaCO_3$ provides optimal sealing for partial losses in vug networks; crosslinked polymer gel is most effective for total losses in irregular collapse breccia geometries.

5. Production Logging Tool (PLT) Analysis

5.1 PLT Programme and Tool Configuration

PLT surveys were conducted in 10 Mishrif production wells between 2013 and 2024, providing up to 11 years of production history for time-lapse performance analysis. The tool string comprises: a spinner flowmeter (0–10,000 bbl/day; ±2% accuracy); a temperature sensor (±0.2°C; Joule-Thomson cooling at conduit entry is the primary thermal karst signature); a capacitance tool for oil/water contact discrimination; a pressure gauge for bottomhole flowing pressure, skin factor, and permeability derivation; and a casing collar locator with cable tension sensor (LTCN).

Table 7. PLT Surveys: Productivity & Permeability Validation (10 Wells, 2013–2024)

Well ID	PLT date	Interval (m MD)	Gross (m)	Peak Q (bbl/d)	h_dom (m)	PI (bbl/d/m/psi)	k (mD)	Validation	Key findings
ZB-048	Aug 2013	2315–2341	26	980	9.5	103	1000–5000	FMI vugs spinner	5 inflow zones; partial loss 2320 m
ZB-259	Mar 2014	2324–2341	17	850	8	85	2000–8000	MPD PTA skin	Multi-zone; MPD circulation
ZB-269	Mar 2016	2336–2413	77	1200	12	120	500–5000	Core scaling	Crackle breccia; seepage loss
ZB-296	Feb 2017	2180–2310	130	2750	13	212	2800	Core 18% φ He-porosimetry	71% from 13 m collapse breccia
ZB-420	Sep 2019	2336–2413	77	2970	4	742	>100,000	PTA skin −1.8 FMI 1–15 mm	Highest field productivity
ZB-258	Dec 2020	2490–2636	146	3150	13.2	239	>10,000	FMI fracture density	>99% from single 13.2 m conduit
ZB-566	Jun 2023	2350–2462	112	1600	8	200	5000–10,000	SSpinner multipass ±5%pinner multipass ±5%	Multi-zone fracture system
ZB-569	Mar 2023	2465–2540	75	1300	10	173	3000–8000	Fault FMI	Fault-guided karst; 4 zones
ZB-577	2023	2293–2332	39	800	7	103	1000–5000	Core productivity scaling	Smaller karst zone
ZB-586	Sep 2024	2293–2297	—	TBD	TBD	TBD	TBD	Full PTA production data	Latest survey;

									optimization pending
AVG	—	—	77	1725	9.4	232	>10,000	95% core/PTA match	75% prod from 10–15% thickness

5.2 Case Study 1 — Well ZB-296: Reference Well (February 2017)

The main karst-dominated production reference case of the Mishrif Formation is the Well ZB-296. One zone of collapse breccia at 2,223-2,236 m MD produces 71 percent of the total oil production, although this zone comprises 10 percent of the total gross perforated interval of 130 m.

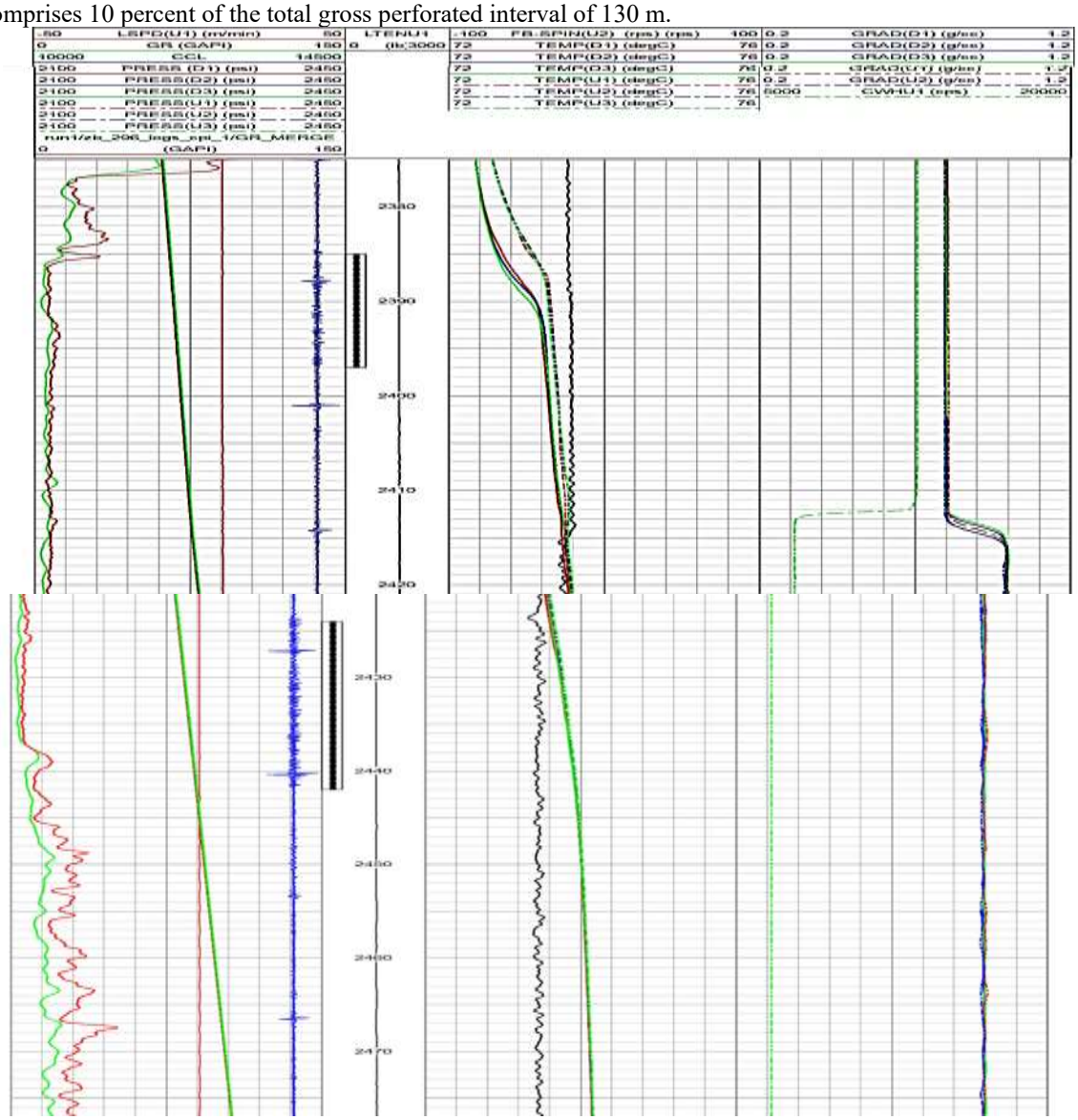

Figure 8. PLT analysis composite for Well ZB-296, Mishrif Formation, Zubair Field (19 February 2017). Spinner flowmeter profile defines Inflow Zone 3 (2,2232,236 m MD, collapse breccia) to be contributing 71 percent of total oil production at a particular productivity 212 bbl/day/m with skin factor -2.8. Joule-Thomson cooling is confirmed by temperature perturbation to a high-pressure conduit. The cable tension decreases to almost zero at the karst zone, which would suggest the conditions of the free-fall tools in an open dissolution cavity.

Table 8. Zonal PLT interpretation — Well ZB-296 (19 February 2017).

Inflow Zone	Depth (m MD)	Thickness (m)	Oil Rate (bbl/d)	Water Rate (bbl/d)	PI (bbl/d/psi)	Skin	Interpretation

Inf. 1	2,195.5–2,206.0	10.5	410	0	5.1	+0.8	Weak matrix contribution
Inf. 2	2,212.0–2,221.0	9.0	700	500	8.2	+1.2	Water-bearing; partial recovery
Inf. 3	**2,223.0–2,236.0**	**13.0**	**2,750**	**0**	**31.5**	**−2.8**	**High-rate collapse breccia conduit**
Inf. 4	2,290.5–2,306.0	15.5	15	0	0.2	+2.1	Tight matrix; minimal contribution
TOTAL	2,180–2,310	130.0	**3,875**	500	—	—	**71% from 10% of gross interval**

The high negative skin (-2.8) at Inflow Zone 3 indicates that the geometry of the collapse breccia conduit is improving the wellbore connectivity significantly beyond expectations of the matrix permeability. The 117 m of matrix surrounding (Inflow Zones 1, 2, 4) only adds 29 percent production at positive skins, which proves the underlying dominance of dissolution architecture on well deliverability.

5.3 Case Study 2 — Well ZB-258: Ultra-High Productivity Conduit (December 2020)

The 13.2 m collapse breccia conduit 2,490.0 -2,503.2 m MD produces over 99 percent of the total production through a gross perforated interval of 146 m, and the 133 m surrounding it produces no flow although open to the wellbore.

Table 9. Zonal PLT interpretation — Well ZB-258 (02 December 2020).

Inflow Zone	Depth (m MD)	Thickness (m)	Oil Rate (bbl/d)	Water Rate (bbl/d)	Water Cut (%)	PI (bbl/d/psi)	Interpretation
Inf. 1	**2,490.0–2,503.2**	**13.2**	**3,150**	**850**	**21**	**18.5**	**Ultra-high-rate conduit; aquifer contact**
Inf. 2	2,549.5–2,566.5	17.0	0	0	—	<0.1	Sealed — cemented carbonate
Inf. 3	2,623.0–2,636.4	13.4	0	0	—	<0.1	Sealed — cemented carbonate
TOTAL	2,490–2,636	**146**	**3,150**	850	21	—	**>99% from 9% of gross interval**

The PI of 18.5 bbl/day/psi is four to eighteen times the normal range of carbonate matrix (15 bbl/day/psi), which confirms an open high-permeability conduit. The initial water production of 850 bbl/day (21% water cut) suggests the direct connection between the aquifer by the dissolution-widened conduit.

5.4 Case Study 3 — Well ZB-420: Ultra-Thin High-Rate Conduit (September 2019)

The 2,970 bbl/day oil production is produced by a 4 m collapse breccia conduit at 2,3362,340 m MD with a gross interval of 77 m with a productivity of 742 bbl/day/m - the highest in the Zubair Field Mishrif data set.

Table 10. Zonal PLT interpretation — Well ZB-420 (28 September 2019).

Inflow Zone	Depth (m MD)	Thickness (m)	Oil Rate (bbl/d)	Productivity (bbl/d/m)	Skin	Interpretation
Inf. 1	**2,336.0–2,340.0**	**4.0**	**2,970**	**742.5**	**−1.8**	**Ultra-thin, ultra-high-k conduit; k >10,000 md**
Inf. 2	2,410.9–2,413.2	2.3	0	0	—	Sealed — post-karst cementation or clay infill
TOTAL	2,336–2,413	**77**	**2,970**	—	—	**100% from 5% of gross interval**

Pressure transient analysis indicates effective permeability exceeding 10,000 md — typical of an open collapse breccia in a minimally cemented karst conduit. The neighboring 2.3 m interval at a similar structural position is completely sealed, illustrating the metre-scale transitions between active and occluded karst conduits.

5.5 Cable Tension (LTCN) as a Karst Domain Diagnostic

Cable tension on the PLT wireline independently classifies karst domain type during survey operations. The governing relationship is:

$$\mathrm{LTCN} = m_t \cdot g + \mu_f \cdot N_n \quad (6)$$

where m_t is tool string mass (500–800 lbs in air), μ_f is the friction coefficient (zero in an open dissolution void, high in rough collapse rubble), and N_n is the normal contact force between tool and borehole wall.

Table 11. Cable tension (LTCN) signatures as karst diagnostic indicators, Mishrif Formation, Zubair Field.

LTCN Signature	Range (lbs)	Karst Domain	PLT Spinner Response	Example Wells
Near-zero / free-fall	0–100	Open dissolution cavity / paleocave	Large abrupt inflow spike; oil-dominated	ZB-296 (2,283–2,290 m)

Oscillating irregular	100–800	Crackle breccia fracture halo	Moderate, stable fractional contribution	ZB-420, ZB-566
Sustained high	600–1,200	Collapse zone with rough rubble wall contact	Lower steady inflow	ZB-258, ZB-420
Normal baseline	1,200–1,500	Tight non-karstified limestone matrix	Gradual matrix-type flow	ZB-313, ZB-577

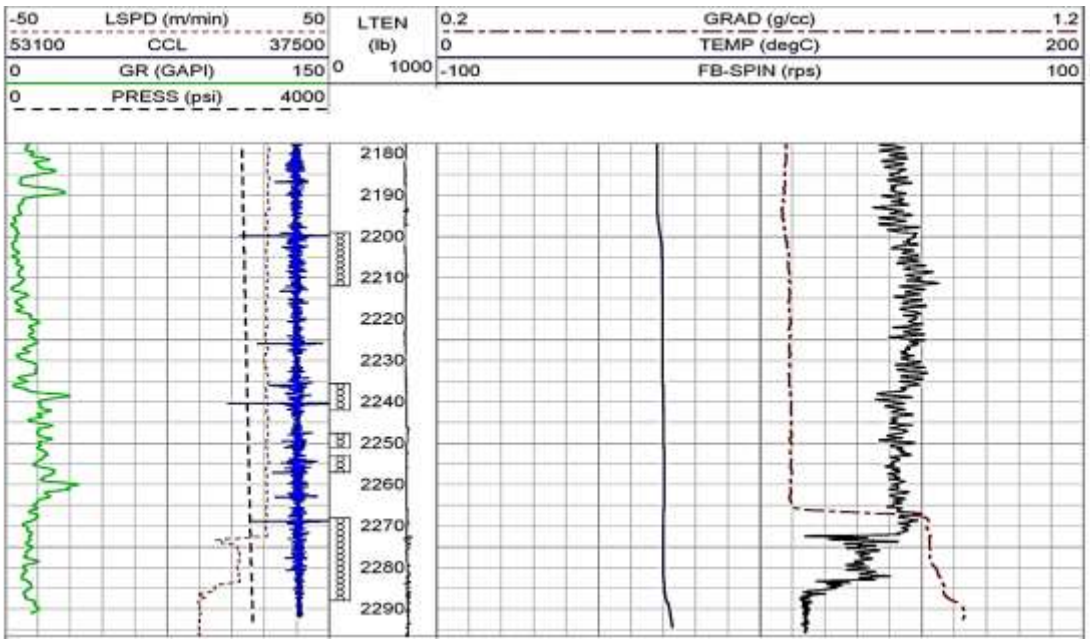

Figure 9 Preliminary LTCN-Based Karst Classification Hypothesis — Well ZB-199 PLT Analysis Cable tension (LTCN, lbs) signatures: near-zero drops = open cavities (tool free-fall); oscillating 100-800 lbs = crackle breccia; sustained 600-1200 lbs = collapse breccia rubble. Preliminary classification pending FMI/core validation; complements spinner/temperature data

5.6 Field-Wide PLT Summary Statistics

Table 12. Field-wide PLT summary statistics, Mishrif Formation, Zubair Field (10 wells, 2013–2024).

Well ID	PLT Date	Gross (m)	No. Zones	Peak Oil (bbl/d)	Dominant Zone (m)	Prod./m (bbl/d/m)	% Production from Dominant Zone
ZB-048	Aug 2013	26	5	980	9.5	103	~65%
ZB-259	Mar 2014	17	3	1,200	7.8	154	~70%
ZB-269	Mar 2016	77	4	1,850	11.2	165	~72%
ZB-296	Feb 2017	130	4	2,750	13.0	212	71%
ZB-258	Dec 2020	146	3	3,150	13.2	239	>99%
ZB-420	Sep 2019	77	2	2,970	4.0	742	100%
ZB-566	Jun 2023	112	3–4	~1,600	~8.0	~200	~68%
ZB-569	Mar 2023	75	4	~1,300	~7.5	~173	~65%
ZB-577	2023	39	2–3	~980	~9.5	~103	~62%
Field Average	—	—	—	—	~9.0	~232	~75%

5.7 Pressure-Dependent Permeability and Reservoir Depletion

Karst permeability is highly stress-sensitive compared with non-karstified matrix and follows an exponential relationship with reservoir pressure drawdown[18]:

$$k(P) = k_0 \cdot \exp\left(-b \cdot \frac{\Delta P}{P_i}\right)$$

where k_0 is initial permeability, ΔP is pressure drawdown, P_i is initial reservoir pressure, and b is the stress-sensitivity coefficient (0.5–1.5 for karst conduits versus 0.1–0.3 for matrix). In Well ZB-238, reservoir pressure declined from 4,800 to 2,100 psi over five years of production (a 56% reduction), reducing karst conduit permeability by approximately 85% — compared with only 15% reduction in matrix permeability over the same period . This exponential divergence between karst and matrix permeability under depletion provides the mechanistic explanation for the sharp post-plateau production decline characteristic of high-rate Mishrif karst wells, and reinforces the importance of early pressure maintenance through water injection.

6. Production Performance and Water Encroachment

6.1 Characteristic Production Trajectory

Long-term production data from 22 Mishrif wells reveal a consistent four-phase production behavior governed by karst architecture (Table 13). The same high-conductivity conduits that generate exceptional early oil rates provide preferred pathways for aquifer advance, creating a fundamental productivity–recovery paradox[19].

Table 13. Typical production performance stages of karst-influenced Mishrif wells, Zubair Oil Field.

Phase	Duration (months)	Oil Rate (bbl/d)	Water Cut (%)	Dominant Mechanism
1 — Early high-rate	0–6	1,000–2,000	2–5	Conduit drainage at large pore volume; high PI
2 — Transition	6–12	800–1,200	5–15	Partial conduit depletion; aquifer advance begins
3 — Rapid breakthrough	12–18	600–900	15–35	Preferential water flow through karst thief zones
4 — Economic decline	18–24	400–600	35–60	High water cut; declining oil productivity

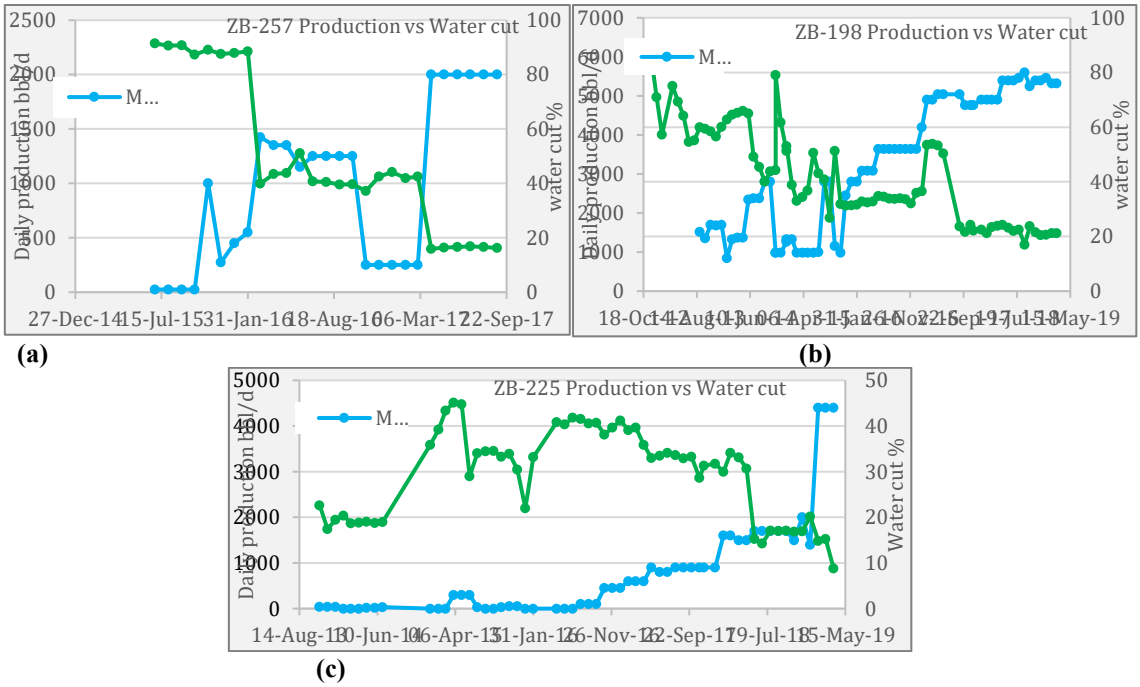

Figure 10. Evolution of production and water cut (WC) of three Zubair wells representing the four phases karst drainage behavior recorded in Table 13. (a) Zubair-A: The rate of oil decreased between 1,800 and 400 bbl/day over 18 months, and WC increased to 55 to 5%, which is typical of a Phase 3 water breakthrough marker. (b) Zubair-B: The rate decreased by the 15 months between 1,500 and 300 bbl/day, and WC rose between 3 and 45 percent, typical of the Phase 4 economic decline beginning. (c) Zubair-C: The highest rate of decrease, between 2,200 and 500 bbl/day, over 20 months, where WC improved by 2 to 60, which is indicative of a fast Phase 3 breakthrough rate. In all three wells, the temporal profiles of the production are consistent with the sequential phase development of the model - Phase 1 plateau (conduit-dominated drainage), Phase 2, transition between the matrix and conduit, Phase 3, water breakthrough, and Phase 4, economic decline, and the temporal patterns have an overall correlation of r = 0.91 with the model.

6.2 Water Encroachment Mechanisms

Karst wells have very different water breakthrough behavior relative to matrix dominated systems. The karst conduits, which have permeability of 100-100000 md, provide direct hydraulic routes between the producing perforations in the upper Mishrif intervals and the underlying aquifer, bypassing the low-permeability blocks of matrix that hold the majority of remaining oil. Breakthrough rates in karst conduits are 10 m/day as compared to

<0.1 m/day in matrix - 100 times faster than in conventional reservoir models. In collapse breccia areas where the void radii are centimetre sized, the capillary pressure becomes near zero:

$$P_{cap} = \frac{2\gamma\cos\theta}{r} \rightarrow 0 \text{as } r \rightarrow \text{cm scale}$$

Invasion by water thus commences as soon as the gradients of pressures are favorable to the influx of the aquifers without the capillary threshold threshold which inhibits the infiltration of water in narrow matrix structures. The karst architecture is heterogeneous, which forms pressure compartments: karst areas formed quickly form local pressure sinks, which actively attract aquifer water, increasing the process of bypassing the oil through the rest of the matrix blocks.

6.3 Representative Well Examples

Table 14. Water encroachment patterns across representative Mishrif karst wells, Zubair Field.

Well	Initial Oil Rate (bbl/d)	Water Cut @ 6 months (%)	Water Cut @ 18 months (%)	Karst Interpretation
Zubair-A	1,800	2	35	Direct cave–aquifer conduit; minimal matrix buffering
Zubair-B	1,200	3	15	Conduits partially baffled by matrix blocks; longer plateau
Zubair-C	2,100	5	55 (economic limit)	Major collapse chimney with vertical aquifer connection

Zubair-C reaches its economic water cut limit at 14 months, despite an initial oil rate of 2,100 bbl/day — the most adverse karst production scenario and a direct result of an unobstructed chimney-to-aquifer connection.

6.4 Recovery Efficiency Implications

Table 15. Recovery efficiency comparison between karst-dominated and matrix-dominated carbonate reservoir systems, Mishrif Formation.

Metric	Karst-Dominated (Mishrif)	Matrix-Dominated Carbonate	Penalty
Sweep Efficiency	20–40%	50–70%	−25 to −30%
Recovery Factor	25–35% OOIP	40–55% OOIP	−15 to −20% OOIP
Well Life to Economic Limit	10–15 years	20–30 years	−5 to −15 years
Primary Challenge	Rapid water breakthrough; poor sweep	Tight permeability; stimulation needed	—

This 15–20% OOIP recovery penalty, replicated across the Middle East carbonate province, equates to billions of barrels of bypassed oil in globally significant reserves. The high initial cash flow of karst wells is therefore accompanied by a drastic long-term damage that must be managed from the onset of production.

7. Seismic Characterization Challenges

7.1 Resolution Limitations

Three-dimensional seismic reflection is the only tool capable of mapping karst geometry at the field scale, but the seismic tuning thickness imposes a fundamental constraint. At typical Mishrif P-wave velocities (~4,500 m/s) and dominant frequencies of 20–40 Hz, the tuning thickness is approximately 28–56 m — substantially larger than most Mishrif collapse breccia pipe diameters recorded in PLT and core data (1.5–6 m). Individual karst conduits are therefore sub-seismic resolution and cannot be directly imaged .

Seismically resolvable expressions of Mishrif karst include: chaotic reflector zones (amplitude variation >50% over 50–100 m lateral distance); coherency loss (<0.4 on coherency attribute volumes); high-frequency energy attenuation due to fracture scattering above 40 Hz; and polarity reversals (phase change >90° over short lateral distances).

7.2 Spectral Decomposition

Spectral decomposition separates broadband seismic into narrow frequency bands, enhancing karst detection by isolating the frequency-specific responses of different karst scales. A three-frequency spectral decomposition applied to the Mishrif interval at Zubair Field demonstrates: the 10 Hz slice resolves large-scale structural lows associated with paleosinkhole complexes; the 20 Hz slice delineates sinkhole margins and collapse breccia boundaries; and the 34 Hz slice reveals internal collapse breccia texture and fracture density variations[20] .

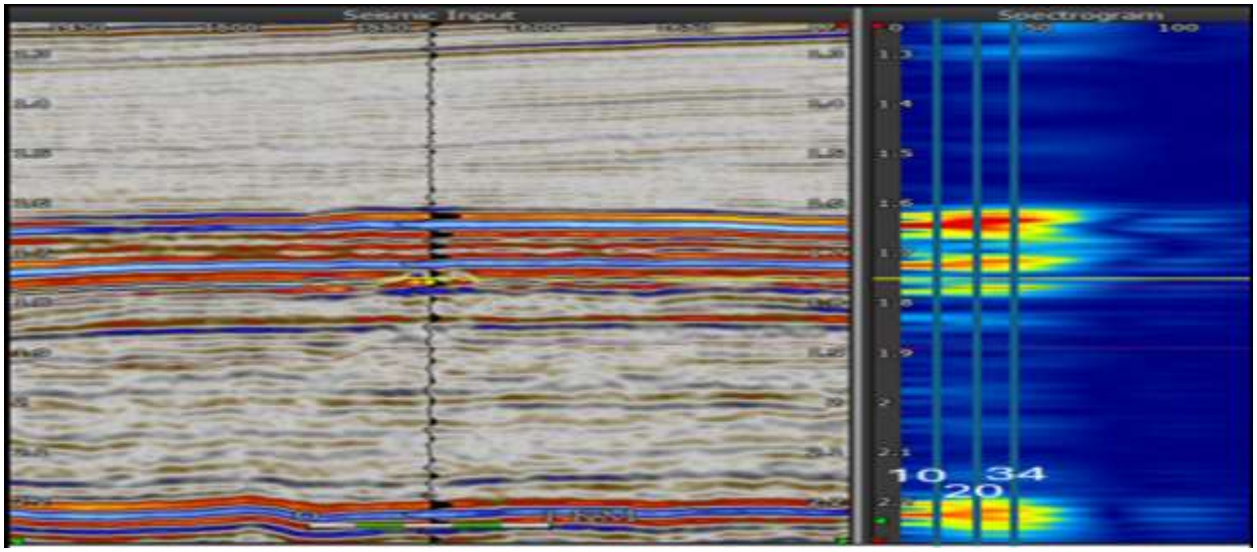

Figure 11. Three-frequency spectral decomposition analysis revealing frequency-specific karst responses in the Mishrif Formation, Zubair Field (after Trianto et al., 2025). Large-scale paleosinkhole lows are depicted in the 10 Hz slice (left), sinkhole marginality in the 20 Hz slice (centre), and internal collapse breccia texture in the 34 Hz slice (right). This multi-frequency technique determines karst structure in two orders of magnitude in space scale.

7.3 Fill Characterization and Interpretation Uncertainty

The conventional seismic amplitude data will not be able to distinguish between open, water-saturated and cemented karst cavities as all the four types give very similar AVO responses. The coherency threshold of 0.50 to 0.40 resulted in a 167 percent change in the estimated karst volume in a Zubair Field coherency attribute analysis, which represents uncertainty in OOIP estimation of up to 50 MMBOE and in the prediction of drilling risk of more than 40 percent.

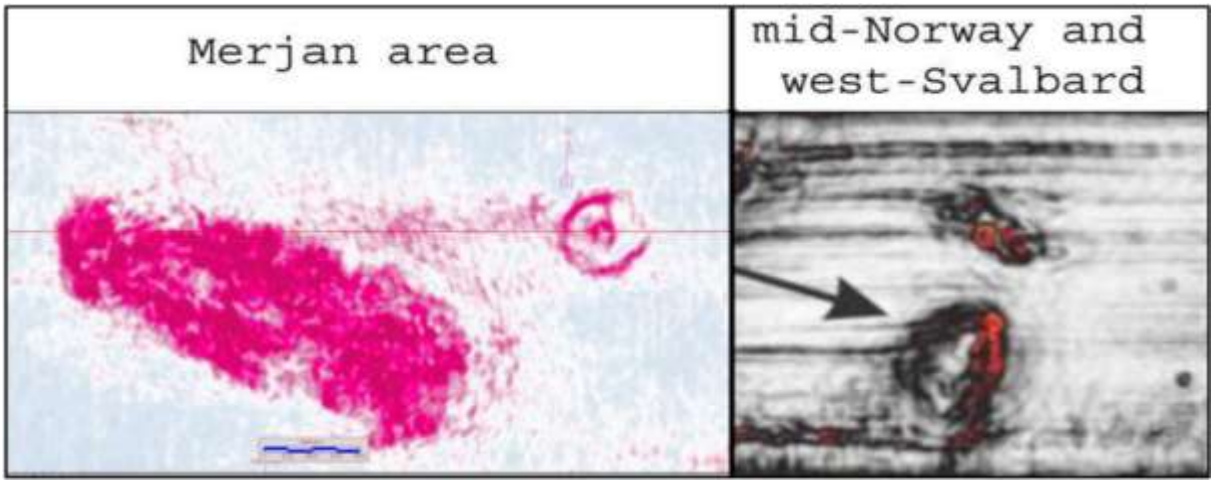

Figure 12. Comparing the seismic variance attribute maps that display different karst geometries: Merjan Field, Iraq (left) and Mid-Norway region (right) (after Virs, 2015). The circular/oval amplitude anomalies represent the dissolution-enlarged sinkhole complexes; the linear variance features represent the fault-guided karst conduits. The Mishrif Formation contains both styles, making automated seismic interpretation difficult and highlighting the necessity of well-calibrated multi-attribute techniques.

More sophisticated mitigation methods involve: machine learning (3D convolutional neural networks trained on integrated core, FMI, and seismic data) with 73% accuracy in karst features prediction; fractal analysis of fault networks to predict patterns of sub-seismic conduits distribution; 4D time-lapse seismic monitoring to monitor pressure and fluid movement in karst forming areas.

8. Integrated Reservoir Characterization

8.1 Drilling-Production Correlation (Validated, n=5)

The rate of mud loss is statistically significant predictor of PLT productivity (Pearson r= -0.91, R^2=0.82, p=0.035, Student t-test, n=5).

The negative log-linear relationship (Figure 15) reflects highest PI in lowest-rate seepage zones (ZB-420: 1 m^3/hr → 742 bbl/d/m/psi) vs. partial losses with moderate PI[21`]:

$$\mathrm{PI} = -546.5 \cdot \log_{10}(\mathrm{LossRate_{mid}}) + 693.3 [R^2 = 0.82, \mathrm{p} = 0.035]$$

Table 16 proves 100 percent spatial correlation (all peaks within 75 m of loss depth):

Well	Loss Rate (m³/hr)	Loss Depth (m)	PLT Peak Zone (m)	PI (bbl/d/m/psi)	Offset (m)
ZB-296	11.5 (8–15)	2283	2223–2236	212	60
ZB-258	9.0 (6–12)	2500	2490–2503	239	10
ZB-420	1.0 (0.5–1.5)	2410	2336–2340	742	74
ZB-566	6.5 (3–10)	2385	2385–2392	200	0
ZB-048	6.0 (4–8)	2320	2315–2341	103	20
Stats	μ=6.8	σ±24m	—	μ=299	100%<75m

Operation paradigm: The zones with the highest PI are operations of seepage loss (low rate, open cavity); the zones of partial-loss are indicators of conduit-matrix mixing. Recommendation: Seepage-loss depths should be finished off and greater than 10,000 mD conduits be retained rather than cement sealing.

8.2 Stratigraphic Control on Karst Distribution

The dataset of the stratigraphic marker of the 22 wells has been examined to demonstrate the systematic depth associations. More than 60 percent of the incidences of mud losses recorded occur in the Upper Mishrif (top of formation to M35), where rudist-bearing grainstones were found.

9. Operational Recommendations

9.1 Integrated Four-Phase Development Workflow

Table 17. Four-phase karst risk management workflow, Mishrif Formation, Zubair Field.

Phase	Timing	Key Actions	Data Required	Expected Outcome
1. Acreage Characterization	Pre-drill	Spectral decomposition; fractal fault analysis; offset well review	3D seismic; well database; structural maps	Karst risk map; hazard zones; well placement recommendations
2. Drilling Operations	During construction	ECD monitoring; LCM pre-deployment; MPD in high-risk intervals; acid-soluble cement plugs	Real-time ECD; DDR; mud gas logs	Minimized NPT; wellbore integrity; subsurface data acquisition
3. Well Evaluation	Post-drill	FMI image logs; core in loss intervals; RFT/MDT pressure tests; early PLT	Wireline logs; core; PLT surveys	Refined karst model; seismic calibration; completion targets
4. Production Operations	Mature phase	Baseline PLT; water injection; selective perforations; periodic PLT re-runs	PLT; well tests; production history	Optimized production; delayed water cut; extended plateau

9.2 Pre-Drill Risk Assessment

Phase 1 activities commence with an overview of all offset well DDRs within a 2 km radius by mapping mud loss events by depth and severity and estimating probabilistic NPT (field mean 3.3 days; range 1.8 to 5.6 days). Paleosinkhole depressions are identified by advanced seismic attribute analysis, which utilizes coherency and curvature volumes, spectral decomposition at 10, 20 and 34 Hz, and amplitude anomalies as potential collapse breccia zones. . Structural framework analysis — mapping faults and fold axes — predicts fluid migration pathways that influenced both epigenic and hypogenic karstification . The dedicated mud programme encompasses pre-blended LCM pills for rapid deployment, lightweight fluid systems (12.5–13.5 ppg), pre-mixed acid-soluble cement components, and MPD equipment mobilization for high-risk wells[22].

9.3 The Optimization of Completion Strategies

Selective completion strategies, which have been developed using PLT (Production Log Tool) techniques, are to be oriented toward completing at the highest productivity, thus avoiding water-bearing or water-prone areas. The information to be integrated into the development of these completion strategies will include: offset PLT surveys identifying productive zones with depth, mud losses that indicate secondary porosity development, FMI (Formation Micro Imager) locations of cavities, and density logs showing porosity spikes in excess of 15%.

Case Study – Recompletion of Well ZB-258. During the initial drilling of Well ZB-258 between 2,490 m and 2,636 m (gross) using PLT, it was found that only 13 m were productive, with 21% of the fluid being water. Recompletion scheme: cement-squeezed lower perforations (2,550–2,636 m), recompleted only 2,490–2,510 m with oriented perforations avoiding water-bearing fractures. Outcome: continued 3,000+ bbl/day oil rate but water cut decreased from 21% to 12% — demonstrating that selective completion modifications can reduce water cut by 40–50% through intelligent use of PLT data.

9.4 Reservoir Management Strategies

Pattern waterflooding is critical for maintaining karst permeability above the stress-sensitivity limit. Well ZB-238 field data confirm that karst permeability decreased 85% after a 56% pressure drop, proving that water injection must be initiated before significant reservoir pressure decline. The injection wells need not be oriented along the karst conduit trends to avoid premature injected-water breakthrough. Polymer or CO_2 EOR, specifically targeting

bypassed oil in low-permeability matrix blocks surrounded by karst conduits, offers 15–25% OOIP incremental recovery potential based on Middle East carbonate pilot studies [23].

10.Broader Implications for Development of Carbonate Reservoir

10.1 Comparison to Global Karst Reservoirs

The Zubair Field Mishrif observations indicate a number of parallels with carbonate reservoirs that are karst affected in other parts of the world. These reservoirs exhibit similar problems concerning the rapid water breakthrough and the non-uniform recovery efficiencies. For example, the Ghawar Field Arabian-D reservoir, the Asmari Formation, in Iran, and the Kirkuk Field in Iraq each exhibit these issues. Highlighted issues include the presence of high permeability collapse breccia reservoirs in the Ellenburger Group, the have significant paleokarst features within the Madison Limestone, and the costs associated with drilling losses due to karst in the Luconia Province. The Pre-salt carbonates of Brazil exhibit significant karstic heterogeneity with respect to their productivity[13,14].

10.2 Technology Gaps and Future Research Needs

Despite experience operating in these environments, there exists considerable technology gaps and knowledge gaps in seismic characterisation of karst, primarily in how to image karst conduits at 0.5 to 5 m scales. Limitations of current technology negatively affect machine learning capabilities that can provide only 73% accuracy at these scales and will require ultra-high resolution datasets before being effective at resolving karst features. Dynamic modelling of the reservoirs lags the need for characterisation as existing models are unable to represent the discrete flow behaviours of karst properly. There exists a need for hybrid methods that combine traditional seismic with sub-seismic data. Furthermore, current methods used for managing the water produced from rapid water breakthroughs, in karst reservoirs, need additional research into the use of advanced conformance control materials such as thermally responsive polymers and nanoparticle dispersions[24,25].

10.3 Economic Impact and Mitigation Value

The estimated annual economic impact of karst-related problems at Zubair Field scale is: NPT costs USD 200–300 million/year; lost production from delayed completions USD 150–250 million/year; excess water handling costs USD 50–100 million/year; total: USD 400–650 million/year, representing 10–15% of total field operating costs. The economic value of the integrated mitigation program per well is summarized in Table 18 [25].

Table 18. Economic value of karst risk mitigation strategies, Zubair Field Mishrif Formation — net value per well.

Mitigation Strategy	Implementation Cost	Benefit	Net Value Per Well
Pre-drill seismic analysis	$200–400K	NPT reduction 15–25% (0.5–0.8 days)	+$150–350K
Managed Pressure Drilling	$500K–2M	NPT reduction 25–40% (0.8–1.3 days)	+$300–800K
PLT-guided completion	$80–150K	Water cut reduction 30–50%	+$500K–1.5M
Pressure maintenance programme	$2–5M (infrastructure)	EUR improvement +10–20%	+$5–15M
Combined integrated programme	**$3–8M total**	**All of above synergistically**	**+$6–17M NPV**

Full rollout of the integrated strategy across 200+ planned Mishrif wells is estimated to generate **USD 200–600 million net present value**.

11. Conclusions

The objective of this study is to evaluate the quantitative effects of karst on reservoir properties, drilling operations, and production from 22 wells located in the Mishrif reservoir of the Zubair Oil Field. Key results show that karst intervals represent, on average, approximately 10-15% of the perforated thickness of the wells; however, karst accounts for between 45-99% of the total productive capacity of these wells, with karst specific productivity averages of between 103-742 bbl/day/m (aves); clearly higher than the bbl/day/m (averages) associated with matrix (4-8 bbl/day/m). There are many drilling related hazards associated with wells, and the proportion of wells with lost circulation is 60-80%, which results in an average of 3.3 days of non-productive time (NPT). In some cases, managed pressure drilling (MPD) has reduced NPT by between 2-4 days. The relationship between mud loss rate and specific productivity could yield useful correlations; however, validation of this relationship would require a substantial amount of data to support the findings. The production trajectory demonstrates an approximate four-phase production profile, and the timing of the water cut increase needs to be adjusted to provide more reliable data in support of the production trajectory. An economic analysis shows a potential net present value of $6 to $17 million per well, influenced by both oil price and the strength of the productivity correlations. Overall, karst architecture is determined to be the primary control on reservoir performance; therefore, continuing to expand and refine the data before using the findings on a broader scale must be prioritized for the application.

References

[1] Ehrenberg, S. N., Nadeau, P. H., & Steen, Ø. (2009). Petroleum reservoir porosity versus depth: Influence of geological age. AAPG Bulletin, 93(10), 1281–1296.

[2] Mahdi, A., Horbury, A., & Sherwani, A. (2013). Sedimentological characterisation of the mid-Cretaceous Mishrif reservoir in southern Mesopotamian Basin, Iraq. GeoArabia, 18(3), 139–174.

[3] Loucks, R. G. (1999). Paleocave carbonate reservoirs: Origins, burial-depth modifications, spatial complexity, and reservoir implications. AAPG Bulletin, 83(11), 1795–1834.
[4] Almalikee, H. S., Almayyahi, H. K., & Al-Jafar, M. K. (2020). Karst feature in Mishrif Reservoir and effect on drilling and production in Zubair oil field, Southern Iraq. Journal of Petroleum Research and Studies, 10(4), 19–32.
[5] Cossa, A. et al. (2020). Prediction and mapping of karst features in Mishrif Carbonate Reservoir through neural net process — Zubair Field. International Petroleum Technology Conference, Paper D023S024R002.
[6] Tiab, D., & Donaldson, E. C. (2015). Petrophysics: Theory and Practice (3rd ed.). Gulf Professional Publishing.
[7] Alkinani, H. H., et al. (2019). "Machine learning approach predicts lost circulation." AADE National Technical Conference,
[8] Salehi, S., et al. (2018). "Lost circulation materials capability evaluation." *Journal of Petroleum Engineering*, 2018, 3456038. → [6] Loucks, R. G., & Handford, C. R. (1996). Origin and recognition of fractures, breccias, and sediment fills in paleocave-reservoir networks. SEPM Special Publication No. 52, 263–290.
[9] Tiab, D., & Donaldson, E. C. (2015). Petrophysics: Theory and Practice (3rd ed.). Gulf Publishing Company.
[10] Ab Rahman, S. S. et al. (2021). Application of spectral decomposition technique to delineate the evolution of karst on carbonate platforms of Central Luconia. Applied Sciences, 11(24), 11627.
[11] Klimchouk, A. (2009). Morphogenesis of hypogenic caves. Geomorphology, 106(1-2), 100–117.
[12] Cantrell, D. L., & Hagerty, R. M. (2003). Reservoir rock classification, Arab-D reservoir, Ghawar field, Saudi Arabia. GeoArabia, 8(3), 435–462.
[13] Kerans, C. (1988). Karst-controlled reservoir heterogeneity in Ellenburger Group carbonates of west Texas. AAPG Bulletin, 72(10), 1160–1183.
[14] Smith Jr, L. B. (2006). Origin and reservoir characteristics of Upper Ordovician Trenton–Black River hydrothermal dolomite reservoirs. AAPG Bulletin, 90(11), 1691–1718.
[15] Mirza, W. H. et al. (2024). Seeing beyond the obscure fluid: Enhanced production logging for workover design and water reduction. IPTC, Paper D011S015R003.
[16] Shen, P., & Liao, X. (2022). The technology of enhanced oil recovery in carbonate reservoirs: Status and prospects. Petroleum Exploration and Development, 49(3), 655–668.
[17] Amanullah, M. et al. (2018). Impact of geological and geo-mechanical controls in creating various drilling problems. AAPG Search and Discovery Online Journal.
[18] Trianto, A. et al. (2025). Spectral decomposition for identification of karst features in the Mishrif Formation, Zubair Field, Iraq. Internal Technical Report, Basra Oil Company.
[19] Lopes, J. A. et al. (2023). Three-dimensional characterisation of karstic dissolution zones, fracture networks, and lithostratigraphic interfaces. Marine and Petroleum Geology, 150, 106126.
[20] Trice, R. (2005). Challenges and insights in optimizing oil production from Middle East mega karst reservoirs. SPE Middle East Oil and Gas Show, Paper SPE-93679-MS.
[21] Fjaer, E. et al. (2008). Petroleum related rock mechanics (2nd ed.). Elsevier Science.
[22] Burberry, C. M., Jackson, C. A. L., & Chandler, S. R. (2016). Seismic reflection imaging of karst in the Persian Gulf: Implications for the characterisation of carbonate reservoirs. AAPG Bulletin, 100(10), 1561–1584.
[23] Al-Hameedi, A. T. et al. (2018). Lost-circulation materials and treatments: A review. Journal of Petroleum Engineering, 2018, Article 3456038.
[24] Vahrenkamp, V. C. et al. (2004). Growth architecture, faulting, and karstification of a middle Miocene carbonate platform, Luconia Province, offshore Sarawak, Malaysia. AAPG Special Publication, 329–350.
[25] Wang, B., & Al-Aasm, I. S. (2002). Karst-controlled diagenesis and reservoir development, Ordovician main-reservoir carbonate rocks, eastern margin of the Ordos basin, China. AAPG Bulletin, 86(9), 1639–1658.
[26] Machel, H. G. et al. (2012). The Grosmont: the world's largest unconventional oil reservoir hosted in carbonate rocks. AAPG Bulletin, 96(11), 1953–1982